Materiales de Construcción
Vol. 73, Issue 352, October-December 2023, e328
ISSN-L: 0465-2746
https://doi.org/10.3989/mc.2023.350223

Effect of fiber section shape and volume fraction on the mechanical properties of steel-fiber reinforced concretes

W. He, S. Wu ✉, B. Zhang, Y. Liu, Y. Luo, G. Fu

Northwest A&F University, (Yangling Shaanxi, China)
✉: shoujun_wu@163.com

Received 13 March 2023
Accepted 18 July 2023
Available on line 3 November 2023

ABSTRACT: This study presents the preparation of steel-fiber reinforced concretes (SFRCs) using straight navicular fibers with annular-sector-shaped sections and corrugated fiber with rectangular-shaped sections, respectively. The flexural and splitting tensile strengths of both the respective SFRCs increase with increasing fiber volume fraction, whereas their compressive strengths initially increase, then decrease, and then increase again. For the same fiber volume fraction, the mechanical properties of the navicular fiber-reinforced concrete are superior to those of the corrugated fiber-reinforced concretes. The introduction of steel fiber changes the failure mode of the plain concrete during bending from a typical brittle mode to a bimodal ductile failure mode. As compared to the corrugated fiber, the navicular fiber has stronger interface bonding to concrete and a higher friction resistance to fiber sliding and subsequent pullout. Furthermore, navicular fiber has a higher load-bearing capacity, which makes it more favorable for improving the mechanical properties of plain concrete.

KEY WORDS: Steel-fiber reinforced concrete; Mechanical property; Cross section shape; Failure mode; Strengthening.

Citation/Citar como: He, W.; Wu, S.; Zhang, B.; Liu, Y.; Luo, Y.; Fu, G. (2023) Effect of fiber section shape and volume fraction on the mechanical properties of steel-fiber reinforced concretes. Mater. Construcc. 73 [352], e328. https://doi.org/10.3989/mc.2023.350223.

RESUMEN: *Efecto de la forma de la sección de fibra y la fracción volumétrica sobre las propiedades mecánicas de hormigones reforzados con fibras de acero.* Este estudio presenta la preparación de hormigones reforzados con fibras de acero (SFRCs) utilizando fibras lisas rectas con secciones en forma de sector anular y fibra corrugada con secciones en forma de rectángulo, respectivamente. Las resistencias a la tracción por flexión y división de ambos SFRCs aumentan con el aumento de la fracción de volumen de fibra, mientras que sus resistencias a la compresión inicialmente aumentan, luego disminuyen y luego aumentan nuevamente. Para la misma fracción de volumen de fibras, las propiedades mecánicas del hormigón armado con fibras kisas son superiores a las de los hormigones reforzados con fibras corrugadas. La introducción de fibra de acero cambia el modo de fallo del hormigón simple durante la flexión, de un modo frágil típico a un modo de fallo dúctil bimodal. En comparación con la fibra corrugada, la fibra lisa tiene una unión de interfaz más fuerte con el hormigón y una mayor resistencia a la fricción para el deslizamiento de la fibra y la posterior extracción. Además, la fibra lisa tiene una mayor capacidad portante, lo que la hace más favorable para mejorar las propiedades mecánicas del hormigón en masa.

PALABRAS CLAVE: Hormigón reforzado con fibras de acero; Propiedades mecánicas; Forma de la sección transversal; Modo de falla; Refuerzo.

1. INTRODUCTION

Steel-fiber reinforced concretes (SFRCs) have been widely utilized in deep underground engineering, tunnels, and pavements due to their improved strength, toughness, ductility, and ease of construction, etc. (1-6) In addition to the fiber volume fraction and aspect ratio of length to diameter, the longitudinal shape of the fibers affects the bonding strength between the fibers and concrete, thereby impacting the pullout behavior of fibers and the mechanical properties of fiber-reinforced concretes (7-19). For example, it has been confirmed experimentally that deformed (i.e., hooked and twisted) steel fibers embedded in concrete provide more effective pullout resistance than straight steel fibers (7-14). Furthermore, experimental studies demonstrate that for the same fiber volume fraction, ordinary concrete reinforced with deformed fibers performs better in terms of tensile and flexural strengths than those with straight steel fibers of the same cross-sectional size (7-9), and the same to ultrahigh performance concrete (UHPC) (10-14). Moreover, experimental results reveal that a smaller fiber size provides an evident improvement in the mechanical properties of concretes (7, 15-17). Besides, concretes reinforced with straight steel fibers with smaller cross-sectional dimensions outperforms those with deformed steel fibers in terms of tensile and flexural strengths (7, 14, 16). It should be noted that the fibers involved aforementioned studies have a circular shaped cross section.

Despite the limited number of reported studies,the cross-sectional shape of the fibers is revealed to impact the performance of fiber-reinforced concretes (20, 21). According to Rezakhani et al., for instance, steel fibers with a square-shaped cross-section of 0.91 × 0.91 mm contribute less toward enhancing the compressive strength of concrete than those with circular-shaped cross-sections with diameters of 0.5, 0.2, and 0.16 mm (20). Furthermore, the fiber with a smaller diameter is more favorable for improving the tensile strength and toughness of concrete than that with a larger diameter (20). According to Ushida et al., the compressive and flexural strength of UHPC reinforced with straight steel fibers with a crescent moon-shaped section having an area of 0.13 mm^2 is higher than those reinforced with wavy steel fibers with a square-shaped cross-section with an area of 0.25 mm^2 and lower than those reinforced with hooked steel fibers having a rectangular cross-sectional shape with an area of 0.28 mm^2 (21). Therefore, to analyze the impact of the cross-sectional shape of the fiber on the performance of fiber-reinforced concretes, the fibers concerned must have equivalent section sizes. However, studies on the comparison of the mechanical properties of SFRCs using fibers with equivalent section sizes and various section shapes are lacking. The steel fibers used in steel fiber reinforced concrete in reported studies are mostly with circular or rectangular-shaped section. In China, steel fibers adopted in refractory ceramic castables for industrial kilns are typically with sector annular-shaped section (22-24). It can be expected, for the same cross-sectional area, the surface area per unit length of fibers with different cross-sectional shapes may also be different, and thus lead to the load transfer capacity during pulling been different. However, there are no studies on the mechanical properties of SFRCs using fibers with sector annular-shaped section.

In this study, steel-fiber reinforced ordinary concrete samples are prepared using straight navicular steel fibers with sector annular-shaped section and corrugated steel fiber with a rectangular-shaped section of equivalent section size. Moreover, a comparative study is done to analyze the effects of the fiber section shape and its volume fractions on the compressive strength, splitting tensile strength, and flexural strength of the concretes. A major part of this analysis is focused on exploring the differences in the mechanical properties based on the differences in the two fibers in terms of interface bonding, interface load transfer capacity, and the load-bearing capacity of fibers.

2. RAW MATERIALS AND EXPERIMENTAL PROCEDURE

In the experimental procedure, P.O. 42.5 R ordinary Portland cement (Jidong Cement Co., Ltd., China) and polycarboxylic acid water reducer (Sobute New Materials Co., Ltd., China) are used. As coarse aggregates, gravel with a particle size of 5–20 mm, which has apparent, bulk and stacking densities of 2720 kg/m^3, 1520 kg/m^3, and 1650 kg/m^3, respectively, and water absorption of 0.22%, is used. As the fine aggregate, sand with an apparent density of

Table 1. Gradation of aggregates.

Fine	Sieve size /mm	4.75	2.36	1.18	0.6	0.3	0.15	Sieve bottom
	Cumulative sieve residue /%	2.45	9.99	18.18	39.33	68.86	88.29	100.00
Coarse	Sieve size /mm	-	26.5	19	16	9.5	4.75	Sieve bottom
	Cumulative sieve residue /%	-	0.00	2.70	22.16	85.41	99.36	100.00

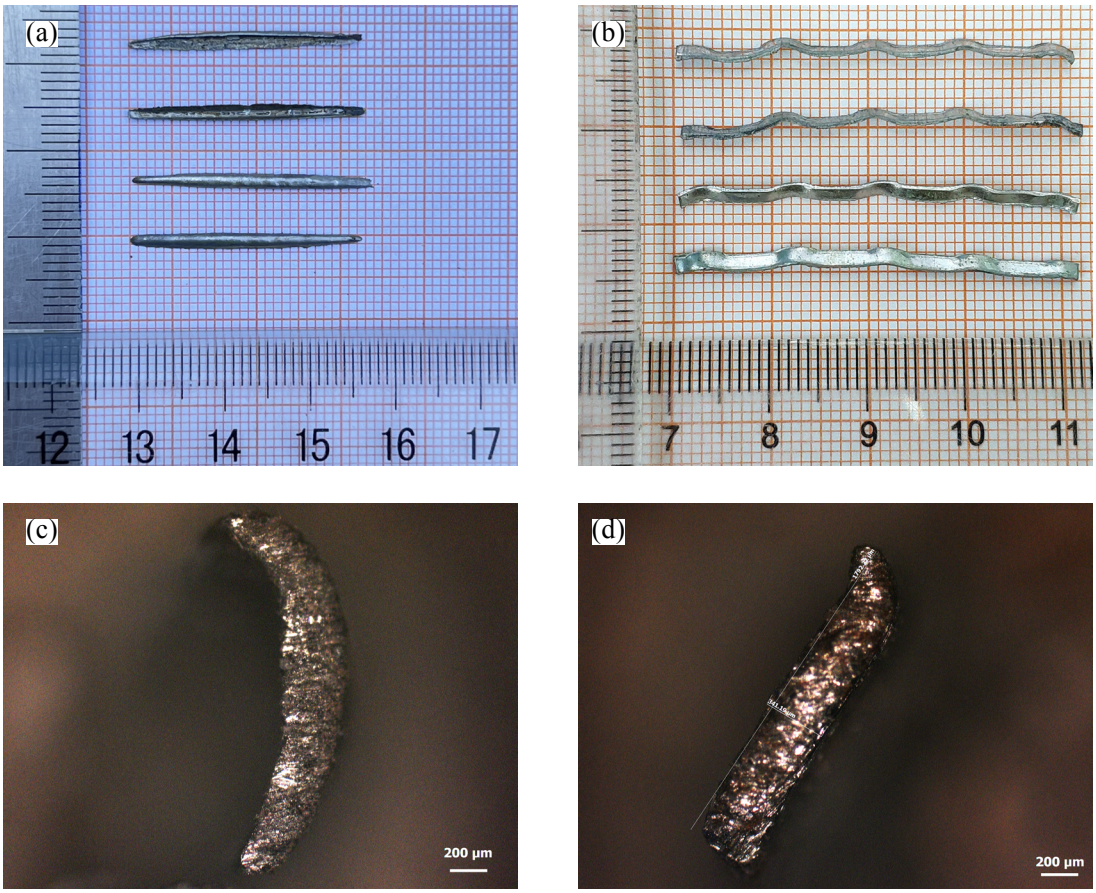

Figure 1. Appearance and section shape of the steel fibers: (a) & (c) Navicular fiber; (b) & (d) Corrugated fiber.

Table 2. Elements of the fibers (in weight %).

	C	Si	Mn	P	S	Ni	Cr	Fe
Corrugated	0.14~0.22	0.3	0.3~0.65	0.045	0.05	-	≤0.030	Balance
Navicular	≤0.30	≤3.00	≤1.50	≤0.04	≤0.03	≤0.45	24.00~27.00	Balance

2640 kg/m^3 is adopted. Table 1 lists the aggregate gradation obtained by the screening test.

In this study, two types of steel fibers are used as reinforcement: the straight navicular steel fiber with an annular-sector-shaped section and the corrugated steel fiber with a rectangular-shaped section. The straight navicular steel fiber with annular-sector-shaped section (446, Zhengzhou Xuanhua Steel Fiber Co., Ltd. China) is produced by extracting the heat-resistant stainless steel melt followed by the rapid quenching method. The corrugated steel fiber with a rectangular-shaped section (CF-35, Beijing Sino-sina Building Technology Co., Ltd. China) is cut from a cold-rolled galvanized iron sheet. Table 2 lists the composition of the fibers (only steel). Before mixing, the navicular fiber is ultrasonically cleaned in a solution of citric acid. Figure 1 shows the appearance and section shape of the two steel fibers, respectively.

The sectional shapes of the two fibers are simplified for further analysis into ideal rectangular and sector annular. Figure 2 depicts a schematic representation of the cross-sectional size parameters of the two fibers. As indicated in the figure, point C represents the section centroid. The x_c-axis and the y_c-axis represent the centroidal axes. The center of the circle corresponding to the annular sector is represented by point O. Table 3 displays the length and the geometric parameters of the fiber sections observed through a microscope (Axio Scope A1, Carl Zeiss Microscopy GmbH, Germany) based on 11 groups of randomly chosen fibers. The diameter of a solid circular section fiber with the same cross-sectional area to a non-cir-

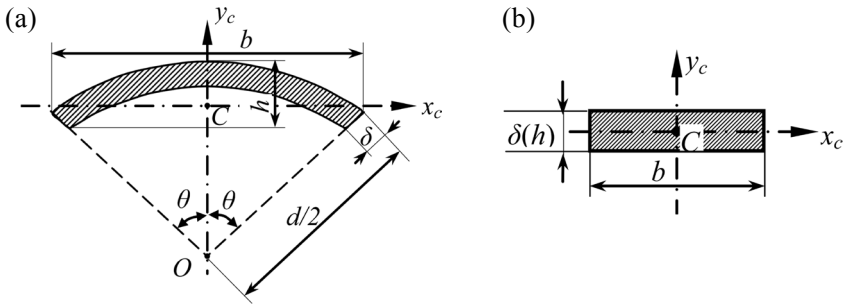

Figure 2. Schematic of simplified section and relevant size parameters of: (a) Navicular fiber; (b) Corrugated fiber.

Table 3. Cross-section size parameters of the fibers.

fiber	Length l/mm	Width b/mm	Thickness δ/mm	Height h /mm	Sectorial angle 2θ/rad	Sectionarea A/mm^2	Section circumference p/mm	Equivalent diameter d_e/ mm	Equivalent aspect ratio
Corrugated	42.76	1.85	0.34	0.34	-	0.648	4.39	0.91	47.09
Navicular	26.79	1.89	0.30	0.62	2×0.734	0.818	5.61	1.02	26.26

cular section fiber is defined as the equivalent diameter of a non-circular section fiber.

The water used for mixing is municipal water from the city of Yangling. Concrete samples with different fiber volume fractions of 0%, 0.5%, 1.0%, 1.5%, and 2.0% were prepared to analyze their impact on the mechanical properties of concrete. The water-to-cement ratio of 0.5 is adopted for each mixture. Table 4 lists the sample numbers and their respective mix proportions.

The compressive and splitting tensile strength testing was conducted on cubes molded with a nominal size of 100 mm×100 mm×100 mm, whereas the three-point bending strength testing was conducted on unnotched prisms that were molded with a nominal size of 100 mm×100 mm×400 mm. The pullout behavior of the steel fibers was measured using 8-shaped specimens with four fibers embedded within the concrete matrix. As depicted in Figure 3 (a), the fiber embedment lengths are fixed at half of the fiber length from the center of the 8-shaped sample. The samples were demolded after casting for 24 h and subsequently cured in a chamber with relative humidity (R.H.) of 95% at 20 °C for 28 days.

The testing of the mechanical properties of the samples is performed by an Instron 1195 machine at room temperature (25 °C and 65% R.H.). As displayed in Figure 3 (b), a uniaxial pullout load is applied on the 8-shaped sample at a loading rate of 0.4 mm/min. The fiber pullout testing was conducted on five samples in each group. The loading rate for the compressive strength test and splitting strength test is 0.4 MPa s^{-1}, while that for the flexural strength test is 0.2 mm min^{-1}. Every test involves the testing of three samples in each configuration. The average of the tested values that were chosen with an error range within 15% is used to calculate the strength under consideration.

Table 4. Sample number and mix proportion of the concretes.

Samples number	water/cement ratio	Water /(kg/m^3)	Cement /(kg/m^3)	Fine aggregate /(kg/m^3)	Coarse aggregate /(kg/m^3)	Water reduce agent /(kg/m^3)	Navicular fiber /(kg/m^3)	Corrugated fiber /(kg/m^3)
F0J0	0.5	180	360	805	1105	2.16	0	0
F5J0	0.5	180	360	805	1067	2.88	38	0
F10J0	0.5	180	360	805	1029	3.60	76	0
F15J0	0.5	180	360	805	991	4.32	114	0
F20J0	0.5	180	360	805	953	5.04	152	0
F0J5	0.5	180	360	805	1067	2.88	0	38
F0J10	0.5	180	360	805	1029	3.60	0	76
F0J15	0.5	180	360	805	991	4.32	0	114
F0J20	0.5	180	360	805	953	5.04	0	152

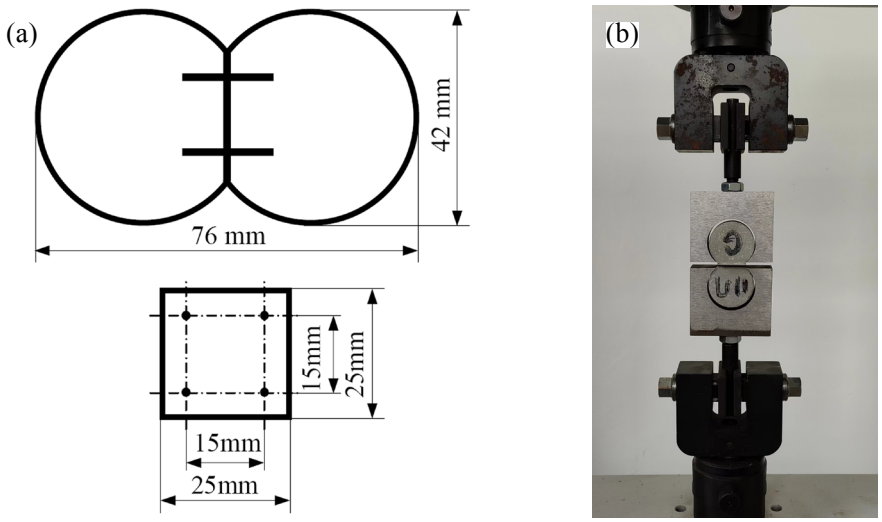

Figure 3. Fiber pull out test (a) schematic of sample geometry; (b) test setup.

The bonding strength of the steel fibers to the concrete is calculated by (13):

$$\tau = \frac{P_{max}}{npL_E} \qquad [1]$$

Equations [2] and [3] are used to determine the splitting strength, $\sigma_{ts,}$ and flexural strength, σ_f respectively (25, 26).

$$\sigma_{ts} = \frac{2P_{max}}{\pi A} \qquad [2]$$

$$\sigma_f = \frac{3P_{max}L}{2bh^2} \qquad [3]$$

where P_{max} denotes the maximum load. p represents the cross-sectional circumference of the fiber; L_E represents the embedment length of the fiber; and n denotes the number of embedded fibers, which, in this study, equals 4. A represents the bearing area of the cubic specimen. L denotes the span during the bending test and is equal to 300 mm. b and h are the width and height of the cross-section of the bending samples, respectively.

3. RESULTS

Figure 4 displays the compressive strength of the SFRCs with different fiber volume fractions. It is observed that when the fiber volume fraction is 0.5%, the compressive strength of both SFRCs increases. This strength decreases as the fiber volume fraction rises to 1.5%, after which it increases again. Moreover, the concrete reinforced with the navicular fiber has a higher compressive strength than that with the corrugated fiber. The compressive strength of plain concrete is 39.5 MPa. However, when the fiber volume fraction is 0.5%, the compressive strengths of the navicular steel-fiber reinforced concrete and that of the corrugated steel-fiber reinforced concrete are 53.8 MPa and 52.6 MPa, respectively. The compressive strengths of navicular steel-fiber reinforced concrete and that of corrugated steel-fiber reinforced concrete, respectively, are 51.9 MPa (enhanced 33.92%) and 44.7 MPa (enhanced 9.11%) when the fiber volume fraction is 2.0%.

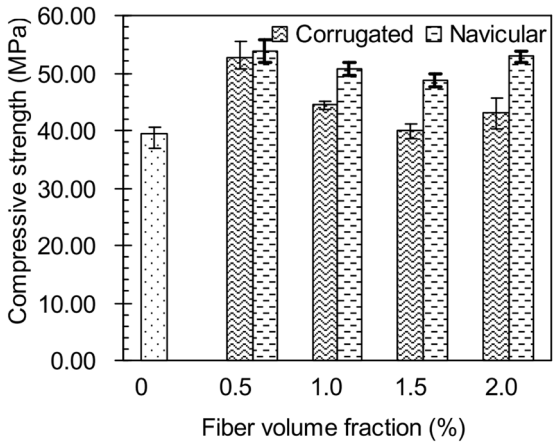

Figure 4. Compressive strength of the steel-fiber reinforced concretes.

Figure 5 shows the flexural strength of the SFRCs with different fiber volume fractions. It is noted that with increasing fiber volume fraction, the flexural strength of both SFRCs increases. Furthermore, for the same fiber volume fraction, the concrete reinforced with navicular fibers has a higher flexural strength than that reinforced with corrugated fibers. Moreover, the flexural strength of the plain concrete

is 6.08 MPa. When the fiber volume fraction is 2.0%, the navicular steel-fiber reinforced concrete and the corrugated steel-fiber reinforced concrete have flexural strengths of 7.90 MPa and 7.23 MPa, respectively, which are 29.93% and 18.91% higher than the plain concrete.

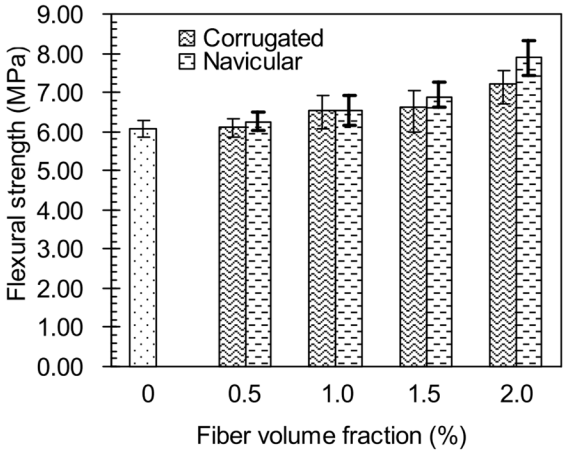

Figure 5. Flexural strength of the steel-fiber reinforced concretes.

Figure 6 shows several typical load-displacement curves of plain and steel-fiber reinforced concretes during bending. The load-displacement curves of these two SFRCs are significantly different from those of plain concrete. The load-displacement curve of the plain concrete during bending demonstrates a typical brittle failure mode that is characterized by the monotonic and rapid increase of the load to the maximum value and then sharply drops off a cliff. The load-displacement curves of both types of SFRC demonstrate a bimodal ductile failure mode. During the entire loading process, the load initially rises monotonically and rapidly to the maximum value and then gradually decreases to a peak valley value. Subsequently, it slowly rises again to a certain peak value and then slowly decreases again until failure. Besides, the maximum load during the bending process and the displacement corresponding to the load dropping to 20% of the maximum load of the fiber reinforced concretes are considerably larger than those of plain concrete. Thus, the incorporation of steel fibers can significantly improve the strength and ductility of concrete during bending. Notably, the load decrement from the maximum value to the peak valley value of the descending stage for the navicular steel-fiber reinforced concretes is less than that for the corrugated steel-fiber reinforced concretes, whereas the load increment from the peak valley value to the peak value of the descending stage is larger. For instance, the maximum load, the peak valley value, and the peak value of descending stage for the navicular steel-fiber reinforced concrete F20J0 are respectively 18.02 kN, 13.84 kN, and 15.35 kN, whereas the respective values are 16.63 kN, 11.53 kN, and 12.23 kN for the corrugated steel-fiber reinforced concrete F0J20. Particularly, the load decrement from the maximum value to the peak valley value of the descending stage for the navicular steel-fiber reinforced concrete F20J0 is 4.18 kN, which is less than the 5.10 kN of the corrugated steel-fiber reinforced concrete F0J20. Meanwhile, the load increment from the peak valley value to the peak value of the descending stage for the navicular steel-fiber reinforced concrete F20J0 is 1.51 kN, which is greater than that for the corrugated steel-fiber reinforced concrete F0J20, which has a value of 0.70 kN. Furthermore, for the same fiber volume fraction, the displacements that correspond to the peak load and the load falling to 20% of the maximum load of the navicular steel-fiber reinforced concretes are larger than those of the corrugated steel-fiber reinforced concretes.

Figure 7 demonstrates the splitting tensile strength of the SFRCs with different fiber volume fractions. The figure reveals that the splitting tensile strength of both types of SFRCs increases with increasing fiber volume fraction. The navicular steel-fiber reinforced concretes have a slightly higher splitting tensile strength than the corrugated steel-fiber reinforced

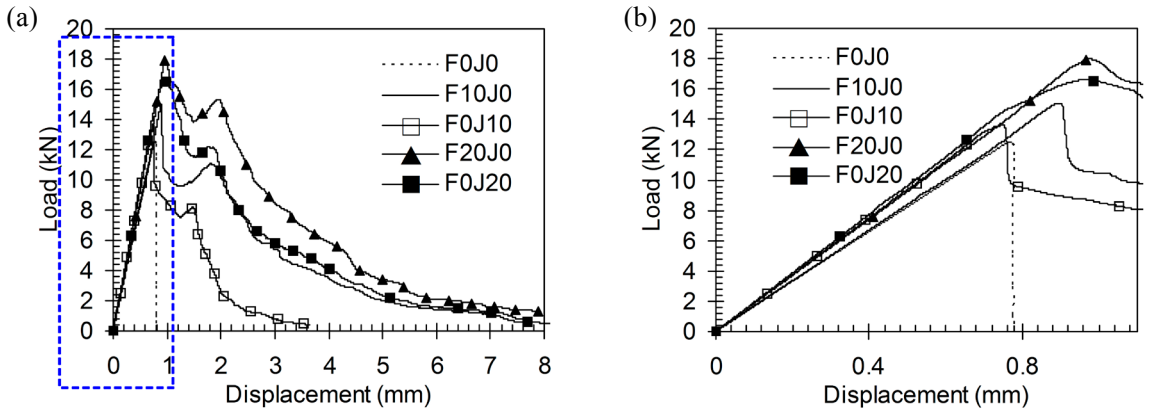

Figure 6. Several typical load-displacement curves of the plain and steel-fiber reinforced concretes during bending.

concretes. Moreover, it is observed that as the fiber volume fraction increases from 0% to 2.0%, the average splitting tensile strength of the concrete reinforced with the navicular steel fiber and the corrugated steel fiber increases from 5.58 MPa to 7.06 MPa and 7.04 MPa, which signifies an increase of nearly 26.52% and 26.16%, respectively.

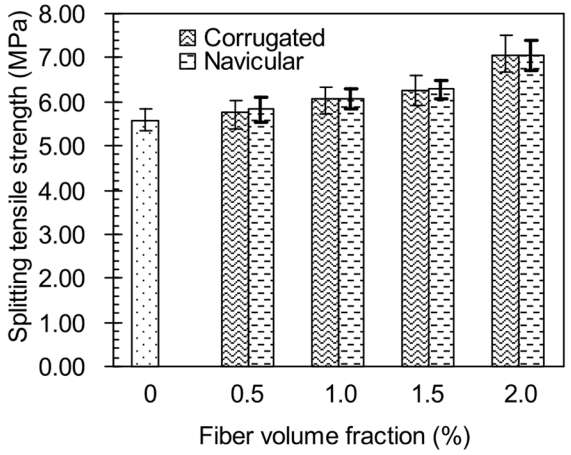

Figure 7. Splitting tensile strength of the steel-fiber reinforced concretes.

Based on the aforementioned findings, it is observed that, though the addition of 2.0% corrugated steel fiber improves the compressive strength of plain concrete only slightly, there is a substantial improvement in both splitting tensile strength and flexural strength. The addition of 2.0% navicular steel fiber can significantly enhance the compressive strength, splitting tensile strength, flexural strength, and ductility of plain concrete. Generally, fiber-reinforced concretes are subjected to bending and compression. Furthermore, the compressive strength of steel-fiber reinforced concretes is significantly higher than the tensile strength. Hence, improving the tensile and flexural properties is of great significance, and the addition of the 2.0% steel fiber is conducive to comprehensively improving the mechanical properties of concrete.

4. ANALYSIS AND DISCUSSION

During compressive loading, the aggregate inside the samples is typically subjected to a compressing effect, while some of the steel fiber could also be subjected to a bending effect in addition to the pressure. The elastic modulus and compressive strength of steel fiber are considerably higher than those of concrete. Hence, the steel fiber is conducive to improving compressive strength. However, as indicated in Figure 8, increasing the fiber volume fraction increases the air content of the concrete, which reduces the compactness of the concrete matrix and consequently weakens the compressive strength. The strengthening and weakening effects will increase with increasing steel fiber content. The compressive strength of SFRC depends on the competition of these two positive and negative effects.

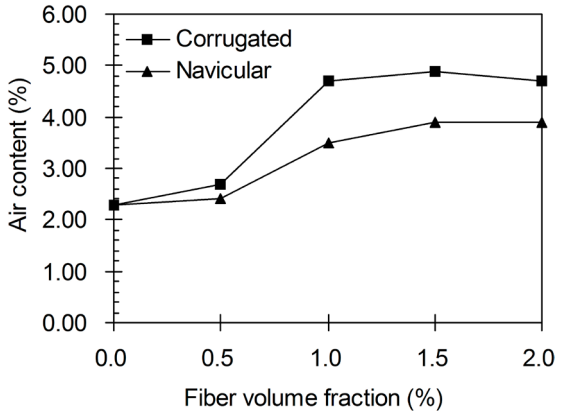

Figure 8. Air content of the steel-fiber reinforced concretes.

Based on the simplified cross-section shapes presented in Figure 2 and the size parameters of the two fiber sections listed in Table 3, the computed values of the moment of inertia of the cross-sectional area about the centroidal axes x_c and y_c for the navicular steel fiber, I_{Fxc} and I_{Fyc}, respectively, are:

$$I_{Fx_c} = \frac{\delta(d-\delta)^3}{8}\left(\theta + sin\theta \times cos\theta - \frac{2sin^2\theta}{\theta}\right) = 13.085\times10^{-3}\ \text{mm}^4 \quad [4]$$

$$I_{Fy_c} = \frac{\delta(d-\theta)^3}{8}(\theta - sin\theta \times cos\theta) = 3.527\times10^{-1}\ \text{mm}^4 \quad [5]$$

The calculated values of the moment of inertia of the cross-sectional area about the centroidal axes x_c and y_c for the corrugated steel fiber, I_{Jxc} and I_{Jyc}, respectively, are:

$$I_{Jx_c} = \frac{b\delta^3}{12} = 6.059\times10^{-3}\ \text{mm}^4 \quad [6]$$

$$I_{Jy_c} = \frac{\delta b^3}{12} = 1.794\times10^{-1}\ \text{mm}^4 \quad [7]$$

Thus, the moment of inertia of the navicular fiber on its centroidal axis is nearly 2.0 times that of the corrugated fiber on the same centroidal axis. This implies that the bending stiffness of the navicular steel fiber is 2.0 times that of the corrugated fiber. When the fiber is subjected to a bending load, the navicular fiber has a larger bearing capacity than the corrugated fiber. Additionally, as presented in Table 3, since the cross-sectional area of the navicular fiber is slightly larger than that of the corrugated fiber, it can withstand a greater axial load (tension and compression). Thus, it can be inferred that for the same fiber volume

fraction, the navicular steel-fiber reinforced concretes can withstand a higher compressive load than the corrugated steel-fiber reinforced concretes and demonstrate superior compressive strength.

On the contrary, as indicated in Figure 8, the air content of both the fiber-reinforced concretes is extremely close to that of the plain concrete at a volume fraction of 0.5%. In this case, the fibers are largely subjected to compression, and due to the random distribution of fibers, relatively few fibers are subjected to bending. Fiber-reinforced concretes exhibit a significant increase in compressive strength since the reinforcement effect of fibers on concrete is greater than the weakening effect. As the fiber volume fraction exceeds 0.5%, a substantial increase is observed in the air content of the navicular fiber-reinforced concrete, from 2.4% to 3.5%, and in the air content of the corrugated fiber-reinforced concrete from 2.7% to 4.9%, respectively. Consequently, the increase in the compactness decrement of the fiber-reinforced concrete is more evident, which implies an enhanced weakening effect. Furthermore, the compressive strength of the fiber-reinforced concretes decreases slightly as the steel fiber volume fraction increases further. When the fiber volume fraction exceeds 1.5%, the air content decreases slightly with steel fiber volume fraction increasing. Therefore, the reinforcement effect of fibers on concrete enhances, whereas the weakening effect diminishes. Hence, the compressive strength of fiber-reinforced concrete increases again.

The tensile and bending strengths of fiber-reinforced composites are mainly attributed to the fibers acting as a bridge across cracks, followed by the pull-out process (27, 28), which is directly influenced by the bonding between the fiber and concrete matrix. A better frictional and stronger adhesive bond along the fiber interface improves the overall mechanical properties of the fiber-reinforced concrete (29). Based on the morphologies of the two kinds of fibers depicted in Figure 1, the surface of the navicular steel fiber is noted to be rougher than the corrugated fiber. Figure 9 illustrates the load-displacement curves of the pull-out test of the navicular and corrugated steel fibers. The peak load for corrugated fiber (about 0.978 kN) is observed to be slightly higher than that for navicular fiber (0.877 kN). However, the two types of fibers achieve their maximum load at a displacement of nearly 1.0 mm. The load-displacement curve of the corrugated fibers sharply drops off a cliff with a displacement of nearly 2 mm after peak load. The load-displacement curve of the navicular fibers demonstrates a clear, gradually decreasing segment following the peak load until failure with a considerably increased displacement of approximately 6 mm, which is indicative of an evident sliding and pulling-off behavior. Notably, the bonding strength of the navicular steel fibers to the concrete (2.92 MPa) is slightly higher than that of the corrugated fiber (2.61 MPa). Furthermore, as depicted in Figure 10, all of the navicular steel fibers are pulled out and adhered with cement paste, while all of the corrugated fibers are broken. The broken section of the bent samples in Figure 11 reveals that the pulled-out navicular steel fibers are also wrapped with a minimal amount of cement paste, whereas traces of cement paste were observed on the surface of the corrugated steel fiber. As listed in Table 3, the navicular fiber has a larger cross-sectional circumference than the corrugated fiber. Therefore, the navicular fiber can withstand a higher friction load than the corrugated fiber. Consequently, the navicular steel fiber is anticipated to have greater friction resistance to fiber sliding and subsequent pullout than the corrugated steel fiber.

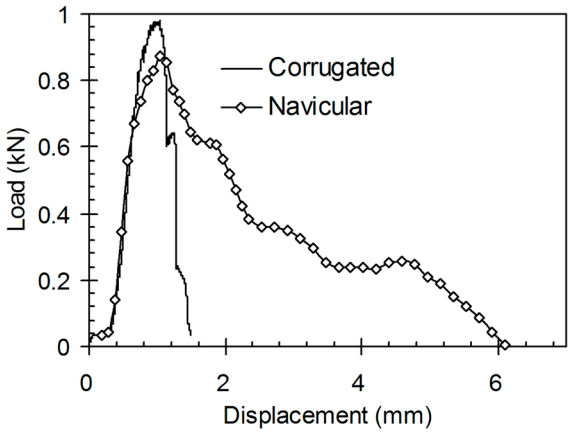

Figure 9. Load-displacement curves of the pull-out test of the steel fibers.

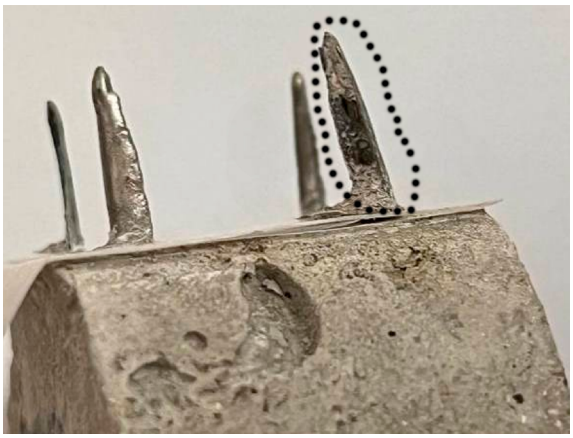

Figure 10. Image of the pulled out navicular steel fibers.

Despite the random orientation of steel fibers in concrete, it can be described as parallel loading direction, perpendicular loading direction, and other directions. The other directions can be viewed as the superposition of the parallel and perpendicular loading directions. The orientation of steel fibers parallel to the loading direction and perpendicular to the loading direction is analysed and numbered as 1 and 2, respectively, for ease of reference. The schematic

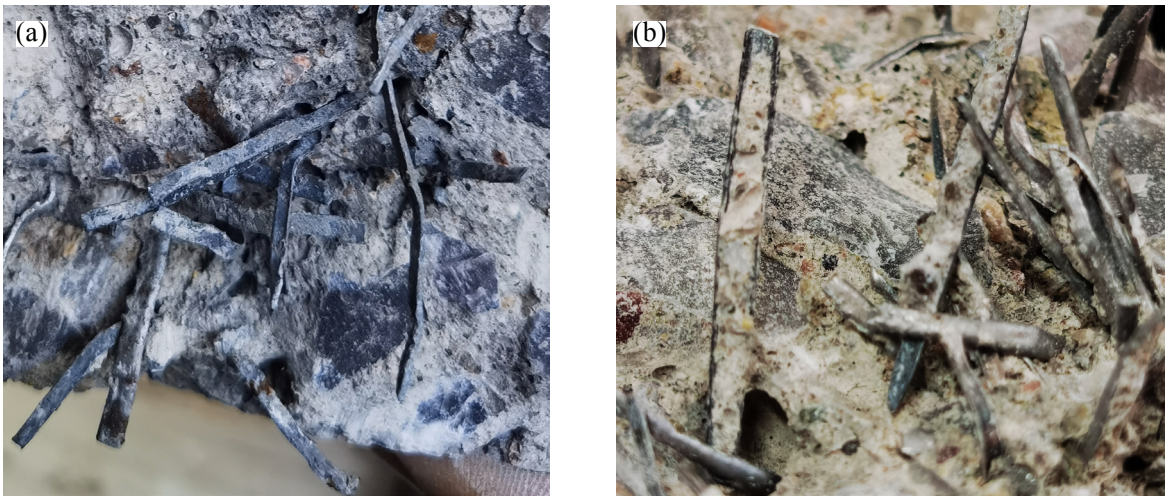

Figure 11. Fibers view on broken section of the bent samples: (a) F0J20; (b) F20J0.

view presented in Figure 12 reveals that near the concrete crack, fiber 1 primarily bears the tensile action (the bridge across cracks), while fiber 2 predominantly bears the tearing action of the concrete separating from the fiber surface. Near the support, fiber 1 largely bears the bending action caused by the shear force perpendicular to the direction of fiber length. Meanwhile, fiber 2 mainly bears the shear action parallel to the direction of fiber length. The aforementioned actions are applied to the fibers by the load transfer at the interface between the fiber and concrete. As compared to the corrugated steel fiber, the navicular steel fiber has a higher load transfer capacity and a higher bearing capacity for the tearing action of the concrete separating from the fiber surface. Furthermore, based on the size parameters of the cross-section of the fibers listed in Table 3, the volume of the individual navicular fiber (21.91 mm^3) is inferred to be considerably smaller than that of the individual corrugated fiber (27.69 mm^3). Therefore, for the same volume fraction, the number of navicular fibers must be higher. Given that the navicular steel fiber has a higher bearing capacity for bending and tensile loading, the navicular steel-fiber reinforced concrete has a higher bearing capacity for bending loads for the same fiber volume fraction. Consequently, for the same volume fraction, the navicular steel fiber has superior strengthening effects than the corrugated steel fiber.

However, as indicated in Figure 6, the gradual decrease in the load after the peak load implies that the load is transferred from the concrete matrix to the steel fibers following the formation of cracks in the concrete matrix. Additionally, the sliding between the fibers and the concrete matrix impedes the rapid expansion and propagation of cracks in the concrete matrix. Moreover, the smaller value of load decrease indicates a greater sliding resistance between the steel fibers and the concrete matrix. Thus, the load transfer effect is better, which implies that the bonding between the steel fibers and the concrete matrix is stronger. Similar to the dislocation movement in crystal materials, when the sliding reaches a certain degree, the sliding will be blocked, causing a gradual increase in the external load (30, 31). The bond between the steel fibers and the concrete matrix will be destroyed as the load increases to a particular extent, resulting in the pullout of fibers and load reduction. Consequently, the pullout of the fibers at different positions decreases the load gradually (32, 33). Therefore, the load increment from the

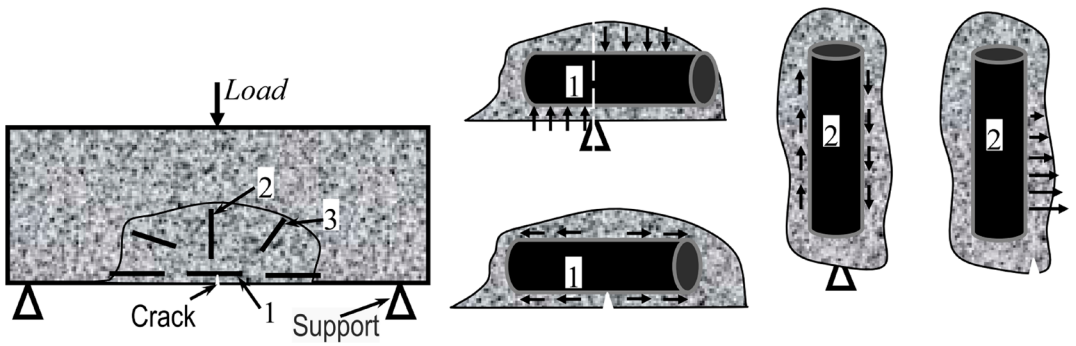

Figure 12. Schematic of stress on fibers with different orientations during bending.

Figure 13. Image of three-point bending induced crack (a) F0J20; (b) F20J0.

peak valley value to the peak value of the descending stage represents the difficulty of fibers pulling out and the ultimate overall cracking. Furthermore, based on the images taken after three-point bending (see Figure 13), it is noted that the navicular steel-fiber reinforced concretes demonstrate more evident multi-deflection crack propagation than the corrugated steel-fiber reinforced concretes. The cracks will deflect when their propagation is hindered by the steel fibers during loading after the formation of the initial cracks in the concrete matrix. The more visible the crack deflection, the more obvious the inhibition effect of fibers on the crack propagation of the concrete matrix, and the greater the energy (load) required for the cracking of the concrete matrix; hence, a better strengthening and ductility-enhancing effect on concrete (34–37). Based on the aforementioned discussion, it can be concluded that, as compared to corrugated steel fiber, navicular steel fiber has stronger interface bonding to concrete, better resistance to cracking and pullout damage, and consequently a better ductility-enhancing effect on concrete (see Figure 6).

The flexural strength and ductility of SFRC are verified to be dependent on the number of steel fibers bearing the tensile action (37). Fiber 1, bearing the tensile action and acting as crack bridges, increases with the increasing fiber volume fraction. Although similar to the compressive strength, an increase in the air content is unfavorable to bonding between the fibers and concrete, which consequently reduces the strength. However, the bonding and shear strengths between the fibers and concrete and the tensile strength of concrete are significantly lower than the strength of the steel fibers. The strengthening effect of fiber is greater than the weakening effect of tensile. Consequently, the flexural strength and ductility of both SFRCs are enhanced with increasing fiber volume fractions.

Bridging across cracks from the fibers inhibits the formation and growth of initial cracks formed in the concrete matrix and is hence beneficial to tensile strength (17, 38–40). As displayed in Figure 11 (a), the corrugated fibers are first straightened in the process of being pulled out and subsequently hinder the expansion of the cracks in the concrete matrix. Therefore, there is retardation for the corrugated fibers to hinder the expansion of the cracks. The navicular steel fibers are straight in the longitudinal direction, which makes them free of the straightening process and thus quickly inhibits the expansion of the cracks in the concrete matrix. However, the larger aspect ratio of corrugated fiber is conducive to the consequent bearing during the propagation of cracks. Consequently, the splitting tensile strength of the navicular steel-fiber reinforced concretes is roughly comparable to that of the corrugated steel-fiber reinforced concretes. Additionally, with an increase in the fiber volume fraction, the fibers bearing the tensile action in the concrete increase. Consequently, the splitting tensile strength of the concrete increases.

5. CONCLUSIONS

The introduction of steel fibers improves the mechanical properties of plain concrete. With increasing fiber volume fraction, the compressive strength of both SFRCs exhibits the same pattern of initially increasing, then decreasing, and then increasing again, and displays the maximum value when 0.5% of steel fiber is added. The flexural strength and splitting tensile strength of both SFRCs increase with increasing fiber volume fraction. For the same fiber volume fraction, the concrete reinforced with navicular steel fibers has superior mechanical properties than those reinforced with corrugated steel fibers.

During bending, plain concrete presents a typical brittle failure mode, while both SFRCs present a bimodal ductile failure mode.

The addition of 2.0% of steel fiber is conducive to comprehensively improving the mechanical properties of concrete.

The difference in improvement in the mechanical properties of the two types of SFRCs arises from the difference

in the characteristics of their cross-section. As compared to the corrugated steel fiber, the rougher surface and the larger section circumference make the navicular steel fiber have a stronger interface bonding to concrete and consequently possess a higher friction resistance to fiber sliding and subsequent pullout. The larger bending stiffness and cross-sectional area contribute to the higher load-bearing capacity of the navicular steel fiber.

ACKNOWLEDGEMENTS

This work was support by the fund of the Natural Science Foundation of Shaanxi Province (2017JQ5113).

AUTHOR CONTRIBUTIONS:

Conceptualization: S. Wu, B. Zhang, G. Fu. Data curation: W. He, S. Wu. Formal analysis: W. He, Y. Liu. Funding acquisition: B. Zhang, G. Fu. Investigation: W. He, S. Wu, B. Zhang, Y. Luo, G. Fu. Methodology: S. Wu, B. Zhang, Y. Luo, G. Fu. Project administration: Y. Luo, G. Fu. Resources: W. He, Y. Liu, Y. Luo. Supervision: S. Wu. Validation: B. Zhang. Visualization: G. Fu. Writing, review & editing: W. He, S. Wu, B. Zhang.

REFERENCES

1. Belletti, B.; Cerioni, R.; Meda, A.; Plizzari, G.A. (2008) Design aspects on steel fiber-reinforced concrete pavements. *J. Mater. Civ. Eng.* 20 [9], 599−607. https://doi.org/10.1061/(ASCE)0899-1561(2008)20:9(599).
2. Kroviakov, S.; Kryzhanovskyi, V.; Zavoloka, M. (2021) Steel fibrous concrete with high-early strength for rigid pavements repair. *IOP Conf. Ser. Mater. Sci. Eng.* 1162 [1], 012008. https://doi.org/10.1088/1757-899X/1162/1/012008.
3. Li, X.; Xue, W.P.; Fu, C.; Yao, Z.S.; Liu, X.H. (2019) Mechanical properties of high-performance steel-fibre-reinforced concrete and its application in underground mine engineering. *Mater.* 12 [15], 2470. https://doi.org/10.3390/ma12152470.
4. Massone, L.M.; Nazar, F. (2018) Analytical and experimental evaluation of the use of fibers as partial reinforcement in shotcrete for tunnels in Chile. *Tunn, Undergr, Space Technol.* 77, 13−25. https://doi.org/10.1016/j.tust.2018.03.027.
5. Wang, X.L.; Fan, F.F.; Lai, J.X.; Xie, Y.L. (2021) Steel fiber reinforced concrete: A review of its material properties and usage in tunnel lining. *Struct.* 34 [5], 1080−1098. https://doi.org/10.1016/j.istruc.2021.07.086.
6. Xu, H.Y.; Wang, Z.J.; Shao, Z.M.; Jin, H.S.; Li, Z.; Jiang, X.Z.; Cai, L.B. (2020) Experimental study on crack features of steel fiber reinforced concrete tunnel segments subjected to eccentric compression. *Mater. Today Commun.* 25, 101349. https://doi.org/10.1016/j.mtcomm.2020.101349.
7. Esmaeili, J.; Andalibi, K.; Gencel, O.; Maleki, F.K.; Maleki, V.A. (2021) Pull-out and bond-slip performance of steel fibers with various ends shapes embedded in polymer-modified concrete. *Constr. Build. Mater.* 271, 121531. https://doi.org/10.1016/j.conbuildmat.2020.121531.
8. Choi, E.; Mohammadzadeh, B.; Hwang, J.H.; Kim, W.J. (2018) Pullout behavior of superelastic SMA fibers with various end-shapes embedded in cement mortar. *Constr. Build. Mater.* 167, 605−616. https://doi.org/10.1016/j.conbuildmat.2018.02.070.
9. Hao, Y.F.; Hao, H. (2017) Pull-out behaviour of spiral-shaped steel fibres from normal-strength concrete matrix. *Constr. Build. Mater.* 139, 34−44. https://doi.org/10.1016/j.conbuildmat.2017.02.040.
10. Wille, K.; Kim, D.J.; Naaman, A.E. (2011) Strain-hardening UHP-FRC with low fiber contents. *Mater. Struct.* 44 [3], 583−598. https://doi.org/10.1617/s11527-010-9650-4.
11. Wille, K.; Naaman, A.E.; El-Tawil, S.; Parra-Montesinos, G.J. (2012) Ultra-high performance concrete and fiber reinforced concrete: achieving strength and ductility without heat curing. *Mater. Struct.* 45 [3], 309−324. https://doi.org/10.1617/s11527-011-9767-0.
12. Wu, Z.M.; Shi., C.J.; He., W.; Wu, L.M. (2016) Effects of steel fiber content and shape on mechanical properties of ultra high performance concrete. *Constr. Build. Mater.* 103, 8−14. https://doi.org/10.1016/j.conbuildmat.2015.11.028.
13. Wu, Z.M.; Khayat, K.H.; Shi, C.J. (2018) How do fiber shape and matrix composition affect fiber pullout behavior and flexural properties of UHPC? *Cem. Concr. Compos.* 90, 193−201. https://doi.org/10.1016/j.cemconcomp.2018.03.021.
14. Sulthan, F. (2020) Influence of steel fiber shapes on fresh and hardened properties of steel fiber reinforcement self-compacting concrete (SFRSCC). *IOP Conf. Ser.: Mater. Sci. Eng.* 849 [1], 012062. https://doi.org/10.1088/1757-899X/849/1/012062.
15. Yoo, D.Y.; Kim, S.; Kim, J.J.; Chun, B. (2019) An experimental study on pullout and tensile behavior of ultra-high-performance concrete reinforced with various steel fibers. *Constr. Build. Mater.*, 206, 46−61. https://doi.org/10.1016/j.conbuildmat.2019.02.058.
16. Yoo, D.Y.; Park, J.J.; Kim, S.W. (2017) Fiber pullout behavior of HPFRCC: Effects of matrix strength and fiber type. *Compos. Struct.* 174, 263−276. https://doi.org/10.1016/j.compstruct.2017.04.064.
17. Liu, Y.W.; Zhang, Z.H.; Shi, C.J.; Zhu, D.J.; Li, N.; Deng, Y.L. (2020) Development of ultra-high performance geopolymer concrete (UHPGC): Influence of steel fiber on mechanical properties. *Cem. Concr. Compos.* 112, 103670. https://doi.org/10.1016/j.cemconcomp.2020.103670.
18. Tai, Y.S.; El-Tawil, S. (2017) High loading-rate pullout behavior of inclined deformed steel fibers embedded in ultra-high performance concrete. *Constr. Build. Mater.* 148, 204−218.https://doi.org/10.1016/j.conbuildmat.2017.05.018.
19. Krasnovsky, R.; Kapustin, D.; Korotkikh, D.; Efishov, L. (2021) Complete diagrams of strain under axial tension of steel-fiber reinforced concrete with different fiber types and content. *IOP Conf. Ser.: Mater Sci. Eng.* 1030, 012013. https://doi.org/10.1088/1757-899X/1030/1/012013.
20. Rezakhani, R.; Scott, D.A.; Bousikhane, F.; Pathirage, M.; Cusatis, G. (2021) Influence of steel fiber size, shape, and strength on the quasi-static properties of ultra-high performance concrete: Experimental investigation and numerical modeling. *Constr. Build. Mater.* 296 [1], 123532. https://doi.org/10.1016/j.conbuildmat.2021.123532.
21. Ushida, K.; Nasir, S.; Uehara, T.; Umehara, H. (2004) Effects of fiber shapes and contents on steel fiber reinforcement in high-strength concrete. *Concr. Res. Technol.* 15 [2], 13−23. https://doi.org/10.3151/crt1990.15.2_13.
22. Feng, H.X.; Jiao, Y.J.; Cao, X.Y.; Liu, J.; Han, Y.H. (2023) Effect of steel fiber on thermal shock resistance of mullite castable. *J. Chin. Ceram. Soc.* 51 [6], 1565−1571. Retrieved from https://qikan.cqvip.com/Qikan/Article/Detail?id=7110021145.
23. Ni, K.X.; Zhang, M.J.; Gu, H.Z.; Huang, A.; Li, H.M.; Shao, Z.J. (2017) Steel fiber toughening mullite-SiC castables for coke dry quenching furnace corbel pillar. *China's Refractory* 26 [1], 24−30. Retrieved from http://www.cnref.cn/EN/Y2017/V26/I1/24.
24. Wang, D.J.; Yu, S.Z.; Hu, Z.Y.; Duan, C.Y. (2021) Development and application of ρ-Al_2O_3 bonded mullite-corundum castables. *Refrac. Lime.* 46 [2], 26−28. Retrieved from http://qikan.cqvip.com/Qikan/Article/Detail?id=7104489221.
25. Ministry of Water Resources, People's Republic of China. SL352—2020. (2021) Test code for hydraulic concrete. Beijing: China Water and Power Press.
26. EN 14651: 2005+A1: 2007, (2008) Test method for metallic fibre concrete—measuring the flexural tensile strength. British Standards Institution, London, UK.
27. Xiong, B.W.; Wang, C.W.; Liu, K.; Wang, Z.J.; Xie, Z.Z.; Zhang, T.; Li, X.T. (2020) Interfacial phase induced

load transfer in short carbon fiber reinforced Nb/Nb_5Si_3 composites. *Mater. Sci. Eng. A*. 799, 140156. https://doi.org/10.1016/j.msea.2020.140156.
28. Sunaga, D.; Koba, T.; Kanakubo, T. (2021) Modeling of bridging law for bundled aramid fiber-reinforced cementitious composite and its adaptability in crack width evaluation. *Mater.* 14 [1],179. https://doi.org/10.3390/ma14010179.
29. Naaman, A.E. (2003) Engineered steel fibers with optimal properties for reinforcement of cement composites. *J. Adv. Concr. Technol.* 1 [3], 241−252. https://doi.org/10.3151/jact.1.241
30. Zhang, N.; Carrez., P.; Shahsavari, R. (2017) Screw-dislocation-induced strengthening–toughening mechanisms in complex layered materials: the case study of tobermorite. *ACS Appl. Mater. Interf.* 9 [2], 1496−1506. https://doi.org/10.1021/acsami.6b13107.
31. Shuang, F.; Dai, Z.; Aifantis, K.E. (2021) Strengthening in metal/graphene composites: capturing the transition from interface to precipitate hardening. *ACS Appl. Mater. Interf.* 13 [22], 26610−26620. https://doi.org/10.1021/acsami.1c05129.
32. Cheng, L.F.; Wu, S.J.; Zhang, L.T.; Xu, Y.D. (2009) Mechanical self-adaptability of a SiC/PyC/SiC composite during oxidation in air. *J. Compos. Mater.* 43 [4], 305−313. https://doi.org/10.1177/0021998308098240.
33. Pereira, E.B.; Fischer, G.; Barros, J. (2012) Direct assessment of tensile stress-crack opening behavior of strain hardening cementitious composites (SHCC). *Cem. Concr. Res.* 42 [6], 834−846. https://doi.org/10.1016/j.cemconres.2012.03.006.
34. Xue, R.; Liu, P.; Zhang, Z.J.; Zhang, N.L.; Zhang, Y.H.; Wang, J.P. (2021) Improvement of toughness of reaction bonded silicon carbide composites reinforced by surface-modified SiC whiskers. *Ceram. Int.* 47 [13], 18150−18156. https://doi.org/10.1016/j.ceramint.2021.03.133.
35. Zando, R.B.; Mesgarnejad, A.; Pan, C.; Shefelbine, S.J.; Erb, R.M. (2020) Enhanced toughness in ceramic-reinforced polymer composites with herringbone architectures. *Compos. Sci. Technol.* 204 [1], 108513. https://doi.org/10.1016/j.compscitech.2020.108513.
36. Zhang, K.; Gao, B.Z.; Gong, M.; Tong, Z.Y.; Fan, J.P. (2022) Design of crack deflection induced high toughness laminated Si_3N_4 ceramics based on hollow oriented one-dimensional microstructure. *Ceram. Int.* 48 [15], 21370−21377. https://doi.org/10.1016/j.ceramint.2022.04.103.
37. Jang, S.J.; Yun, H.D. (2017) Combined effects of steel fiber and coarse aggregate size on the compressive and flexural toughness of high-strength concrete. *Compos. Struct.* 185, 203−211. https://doi.org/10.1016/j.compstruct.2017.11.009.
38. Liu, W.; Luo, L.; Xu, S.L.; Zhao, H.H. (2014) Effect of fiber volume fraction on crack propagation rate of ultra-high toughness cementitious composites. *Eng. Fract. Mech*. 124-125, 52−63. https://doi.org/10.1016/j.engfracmech.2014.03.007.
39. Michels, J.; Christen, R.;Waldmann, D. (2013) Experimental and numerical investigation on postcracking behavior of steel fiber reinforced concrete. *Eng. Fract. Mech.* 98, 326−349. https://doi.org/10.1016/j.engfracmech.2012.11.004.
40. Wang, Z.L.; Shi, Z.M.; Wang, J.G. (2011) On the strength and toughness properties of SFRC under static-dynamic compression. *Compos. Part B-Eng.* 42 [5], 1285-1290. https://doi.org/10.1016/j.compositesb.2011.01.027.